Desalination and Water Treatment
www.deswater.com

doi: 10.5004/dwt.2019.23741

151 (2019) 230–241
May

Adsorption-desorption behavior of silver ions on stainless steel as a proxy for disinfection of domestic hot water

Na Li[a], Xing Li[a,*], Yanling Yang[a], Yongwang Liu[a,b], Li Zhao[b], Zhiwei Zhou[a,*]

[a]*College of Architecture and Civil engineering, Beijing University of Technology, No. 100 Xi Da Wang Road, Chao Yang District, Beijing 100124, China, Tel. +86 13911887848; Fax: +86 10 67391726; emails: lixing@bjut.edu.cn (X. Li), hubeizhouzhiwei@163.com (Z. Zhou), lina19941128@163.com (N. Li), yangyanling@bjut.edu.cn (Y. Yang), 15201227605@163.com (Y. Liu)*
[b]*China Architecture Design Group, Beijing, 100044, China, email: zhao-lee@263.net (L. Zhao)*

Received 12 June 2018; Accepted 1 January 2019

ABSTRACT

The water quality of domestic hot water can be controlled by disinfection with silver ions (Ag^+). In order to maximize the antibacterial effect of Ag^+ and at the same time ensure the water is safe for human use, the adsorption and desorption properties of Ag^+ onto 304 stainless steel (SS) was studied. The effects of the initial Ag^+ concentration, the contact time, and the water temperature on the adsorption process were examined. The antibacterial properties of SS adsorbed with Ag^+ (SS-Ag) were also investigated. The results showed that with an increase of the Ag^+ concentration, water temperature or adsorption time, the equilibrium adsorption capacity increased gradually, and the adsorption process reached equilibrium after 72 h. Adsorption kinetic studies showed that the adsorption of Ag^+ on SS was best described by the pseudo-second order model. The adsorption isotherm data fitted well in the Langmuir isotherm model at 45°C (R^2 = 0.9894), which indicated that the adsorbed silver forms a monolayer on the SS. The thermodynamic modelling indicated that adsorption occurred by an endothermic reaction that occurred spontaneously under high temperature conditions. Elution was impossible with ultra-pure water and tap water was inefficient to desorb the Ag^+ from SS. It can be inferred that the shear action of a water flow inside a water pipe would not remove large amounts of adsorbed Ag^+, so that adsorbed Ag^+ can maintain its antibacterial properties for extended periods. Solutions of sodium thiosulfate or thiourea could effectively desorb Ag^+ from the SS surface, and near to complete desorption (98.35%) was obtained with a 2 mg/L sodium thiosulfate solution. Antibacterial experiments indicated that the SS-Ag could inhibit the biofilm formation and effectively reduce the risk of biofilm pollution. The results presented here provide a theoretical basis for the use of silver in hot water supplies using SS pipes for disinfection purposes.

Keywords: Metal pipe; Adsorption; Silver nitrate; Isotherm and kinetics; Biofilm inhibition

1. Introduction

Domestic hot water is a daily necessity for most people, and even needs stricter quality and sanitary requirement than cold water [1]. Elevated temperature and a relatively long hydraulic retention time provide favorable conditions for bacteria to grow, which may lead to serious safety problems [2]. It has been reported that the heterotrophic plate counts (HPC) in hot water was higher than in cold water, and the number of bacteria in biofilms inside hot water pipes was five-fold higher than those found in cold water pipes [2]. Borella et al. [3] determined hot water contamination by *Legionella* and *Pseudomonas* species in a cross-sectional multicentric survey in Italy, and reported

* Corresponding authors.

Legionella spp. in 22.6% and *Pseudomonas* spp. in 38.4% of 146 samples. Biological contamination of hot water systems in a domestic setting is probably widespread, requiring necessary measures to ensure the safety of hot water.

Conventional drinking water disinfection methods include chlorine, chlorine dioxide, chloramine, UV, etc. However, there are many problems in applying them directly to domestic hot water due to the difference of water quality and operating conditions. Chlorine based disinfection methods efficiently kill microorganisms, but may produce harmful carcinogenic disinfection byproducts (DBPs) [4]. Moreover, the consumption rate of chlorine and the amount of DBPs increased with the rise of temperature, which may eventually lead to pollution again [5]. Chlorine dioxide and chloramine disinfection also have similar by-product problems [6]. UV has good disinfection effect on bacteria, but it needs to be combined with other treatment methods because the irradiation effect cannot be maintained throughout distribution system. Therefore, it is important to re-evaluate conventional disinfection techniques, and innovate new approaches to obtain safe domestic hot water.

Disinfection by means of silver ions (Ag^+) is an effective technology that can be applied to domestic hot water. It not only effectively kills microbes, but also inhibits the growth of biofilms on the inner surfaces of the water supply pipes. Disinfection with 0.04 mg/L Ag^+ at 40°C for 30 min can effectively kill a population of 2.0×10^2 CFU/ml *E. coli* [7]. Due to its broad spectrum of antimicrobial activity at low concentrations, with bacteriostatic and bactericidal effects, antibacterial materials containing Ag^+ have developed rapidly [8,9]. Previous studies have shown that Ag-zeolite and activated carbon with silver-coated composites are strongly antibacterial against *E. coli*, and chitosan–nylon-6 blended membranes containing Ag^+ were active against *E. coli* and *S. aureus* [10–13]. With the development of nanotechnology, silver nanoparticles (AgNPs) have been widely investigated in water disinfection in recent years. Direct application of AgNPs suffers the disadvantage of their tendency to aggregate in aqueous media that gradually reduce antibacterial efficiency during long-term use [14]. AgNPs containing materials have drawn considerable interest from scientists for water disinfection due to their high antibacterial activity and cost effectiveness, which can be used as filter materials, adsorbents and so on [15].

Thus far, the adsorption characteristics of Ag^+ were mainly studied for porous materials at room temperature. Limited knowledge is available on adsorption of Ag^+ on metal pipe inner surfaces, especially at elevated temperatures. Both Ag^+ and AgNPs containing materials had great antibacterial effect. However, most of the antibacterial materials were mainly used for primary disinfection of water rather than the guarantee of water quality during the supply process. The content of Ag^+ in the drinking water needs to be strictly controlled, and must not exceed 0.05 mg/L according to drinking water hygiene standards in China, although in emergency situations it may be necessary to increase the Ag^+ concentration beyond this limit to apply shock disinfection and remove biofilm growth inside pipes. Ag^+ adsorption generally occurs on the metal pipe wall and biofilms also adsorb silver during disinfection, especially when applied at high concentrations or high temperature. A study by Nadia et al. [16] reported that at high Ag^+ concentrations the biofilm adsorption capacity was easily exceeded and biofilm development was inhibited. Hot water pipes are often made of 304 stainless steel (SS). The objective of this study was to examine the adsorption isotherm, kinetics and thermodynamic model of Ag^+ adsorption and it's desorption behavior at 45°C on 304 SS surfaces. The antibacterial properties of SS adsorbing Ag^+ (SS-Ag) were also investigated. The findings offer a reference for optimal application of Ag^+ disinfection technology in domestic hot water systems.

2. Materials and methods

2.1. Materials and Chemicals

In this study, 304 SS was provided by a steel plant in Kunming, China. A stock solution of 1.0 g/L silver nitrate ($AgNO_3$) was diluted with deionized water to the needed concentrations. All reagents used in the study were of analytical grade.

2.2. Adsorption experiments

Before the experiment, the surface of 304 SS samples was sanded with sandpaper to remove impurities, cleaned in an ultrasonic cleaner with ultra-pure water for 20 min, air-dried for 1 h, and finally stored in a desiccator at room temperature. For adsorption experiments, SS samples were incubated under agitation (150 r/min) in a solution containing Ag^+ at a controlled temperature of 45°C (318 K). The applied Ag^+ concentration was varied (0.4, 0.6, 0.8, 1.0, and 1.2 mg/L) as well as the temperature (298, 308, 318, 328, and 338 K). Experiments were performed in triplicate and average findings are reported.

The adsorption capacity at a given time (q_t) and at the state of equilibrium (q_e), the percentage removal of silver at a given time (R_t) and at the state of equilibrium (R_e) were calculated using Eqs. (1–4):

$$q_t = \left[\left(C_0 - C_t\right)\cdot V\right] / S \tag{1}$$

$$q_e = \left[\left(C_0 - C_e\right)\cdot V\right] / S \tag{2}$$

$$R_t = \left[\left(C_0 - C_t\right)\cdot 100\%\right] / C_0 \tag{3}$$

$$R_e = \left[\left(C_0 - C_e\right)\cdot 100\%\right] / C_0 \tag{4}$$

where q_t is the amount of adsorbed silver over time t (mg/m^2), q_e is the mass of adsorbed silver at equilibrium (mg/m^2), C_0 is the initial concentration of silver in the aqueous solution (mg/L), and C_t and C_e are the concentration of silver after time t and at equilibrium, respectively (mg/L). V is the volume of solution (L), S is the effective adsorption surface area of the used 304 SS samples (m^2).

The experimental data were fitted using different kinetic models and equilibrium models. Model equations and constants are listed in Table 1.

Table1
Kinetic and isotherm models used for data analysis

Models	Equations	Parameters	Remarks
Pseudo first-order	$\log(q_e - q_t) = \log q_e - \frac{K_1}{2.303}t$	K_1	K_1 (h^{-1}) is the pseudo first-order rate constant
Pseudo second-order	$\frac{t}{q_t} = \frac{1}{K_2 q_e^2} + \frac{t}{q_e}$	K_2	K_2 (m^2/mg·h) is the pseudo second-order rate constant
Elovich	$q_t = \frac{1}{\beta}\ln(\alpha\beta) + \frac{1}{\beta}\ln(t)$	α β	α (mg/m^2·h) is the initial adsorption rate and β (m^2/mg) is the desorption rate
Intra-particle diffusion	$q_t = K_{id}t^{0.5} + I$	K_{id}	K_{id} (mg/m^2·$h^{0.5}$) is the intra-particle diffusion rate constant and I is the proportional to the boundary layer
Langmuir	$\frac{C_e}{q_e} = \frac{C_e}{q_{max}} + \frac{1}{b \cdot q_{max}}$	b q_{max}	b (L/mg) is the Langmuir constant and q_{max} (mg/m^2) is the maximum adsorption capacity
Freundlich	$\log q_e = \log K_f + \frac{1}{n}\log C_e$	K_f n	K_f ($mg^{1-(1/n)}L^{1/n}m^2$) is the Freundlich constant and n is the heterogeneity factor
Temkin	$q_e = B\ln K_t + B\ln C_e$	K_t B	K_t (L/m^2) is the equilibrium binding constant corresponding to the maximum binding energy and B (J/mol) is the constant related to the heat of adsorption
Dubinin-Radushkevich	$\ln q_e = \ln q_d - B_d\varepsilon^2$	q_d B_d ε	q_d (mg/m^2) is the theoretical maximum isotherm saturation capacity, B_d (mol^2/J^2) is D-R isotherm saturation capacity, ε (KJ/mol) is Polanyi potential

2.3. Desorption experiments

Following adsorption, the SS samples were dried at room temperature and then used in desorption experiments. Ultra-pure water, tap water, 0.1 mol/L sodium thiosulfate ($Na_2S_2O_3$) and 1% thiourea (CH_4N_2S) were used as eluents. Desorption experiments were performed under agitation (150 r/min) and at a constant temperature (45°C). The samples were desorbed for 6, 12, and 24 h, and the desorption rate (R_{des}) was calculated based on Eq. (5).

$$R_{des} = Ag_{sol} \cdot 100\% / Ag_{sor} \quad (5)$$

where Ag_{sol} is the silver content in solution after desorption (mg), and Ag_{sor} is the silver content on sorbent (mg).

2.4. Antimicrobial experiments

The growth of biofilm was examined in biofilm annular reactor (BAR), which was used to simulate conditions relevant to domestic hot water distribution systems. Two BARs accommodate 18 removable coupons (SS-Ag for R_1, SS for R_2), respectively. The effluent from another biofilm-matured reactor was used as the influent of R_1 and R_2 to simulate biofilm growth under condition of water pollution. The biofilm formation on SS-Ag and SS coupons were evaluated by collecting the samples at different time intervals over a period of 30 d. The biofilm growth inhibition property of SS-Ag was studied through standard plate count method, including total number of bacterial, *E. coli* and HPC. Biofilm growth on SS was performed as control. The efficacy of antibacterial activity of SS-Ag was determined by Eq. (6):

$$\text{Antibacterial efficacy } (\%) = \left[\left(N_{SS} - N_{SS\text{-}Ag}\right) / N_{SS}\right] \times 100 \quad (6)$$

where N_{SS} and $N_{SS\text{-}Ag}$ are numbers of viable cells in biofilms scraped off SS and SS-Ag coupons, respectively.

2.5. Analytic methods

The concentration of Ag^+ was determined by an atomic adsorption spectrophotometer (AAS, vario6, Jena, Germany). The surface morphology was analyzed by scanning electron microscopy (SEM, SU-8010, Hitachi, Japan), which was performed at coarse vacuum with an accelerating voltage of 15kV. The elemental composition and content were analyzed using an energy dispersive spectrometer (EDS). X-ray photoelectron spectroscopy (XPS, PHI Quantera SXM, ULVAC-PHI, Japan) was used to determine the elemental composition and valence state. The analyzer pass energy was 280 ev for survey spectra and 55 ev for high resolution spectra. The chemical state of silver is difficult to determine using the sole Ag_{3d} binding energy, which varies with the particle size and may shift due to charging effects. To overcome this problem, the modified Auger parameter was used. The standard method (Standard Test Method for Hygienic Standard of Drinking Water) was used to determine the total number of bacteria and membrane filtration method was used to determine the number of *E. coli*. HPC were performed using a spread plate technique on R2A agar. R2A plates were incubated at 22°C ± 1°C for 7 d.

3. Results and discussion

3.1. Characteristics of the stainless steel before and after silver adsorption

3.1.1. Microscopic analysis of the treated samples

After SS samples were allowed to adsorb silver by submerging them in $AgNO_3$ solution for 24 h, their surface became less shiny, probably due to the formation of an oxide film. SEMs were produced before and after adsorption of silver and magnifications of 2,000 and 5,000 times are shown in Fig. 1. Prior to adsorption, the surface of SS was relatively smooth and adsorbed substances were not observed. Following adsorption, the surface was less smooth and adsorbed substances can be observed on the surface, with higher amounts located at the cracks. The emergence of electron-dense areas could be inferred as the result of silver adsorption.

To verify whether the electron dense part on the surface of SS contained silver, EDS analysis was performed. The results of three such areas are shown in Fig. 2. The analyzed areas contained high levels of Fe, Cr, Ni, and C, and relatively small amounts of Si, Mn, S, and some other elements. The analysis results had a high degree of accuracy and the results were in line with the 304 SS standard element content composition, except for C. The latter element is probably due to surface contamination.

An Ag peak was clearly visible. There was more silver adsorbed on surfaces with large depressions (e.g. area 2) and cracks (area 3), where 14.2% and 1.8% Ag was detected, respectively. Based on the SEM images before and after adsorption (Fig. 1), some Ag was expected to be adsorbed to smooth surface areas as well, but for one such surface (area 1) no Ag was detected; possibly any adsorbed silver present here remained under the detection limit of EDS.

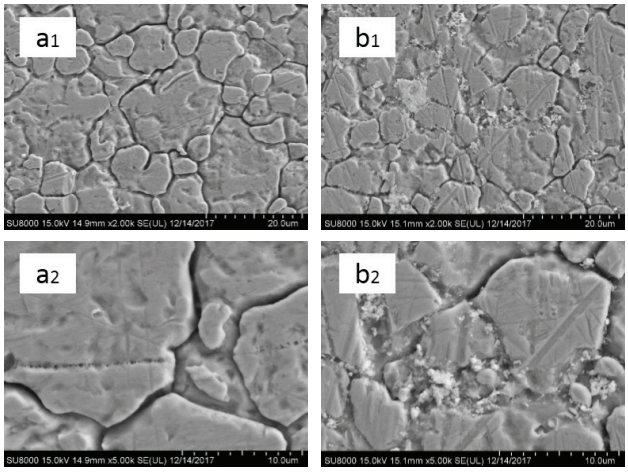

Fig. 1. SEM images of SS: before adsorption (a(1) and a(2)) and after adsorption (b(1) and b(2)) following exposure to a silver nitrate solution with Ag^+ concentration of 1.0 mg/L and temperature of 45°C. Magnification 2,000x (top) and 5,000x (bottom).

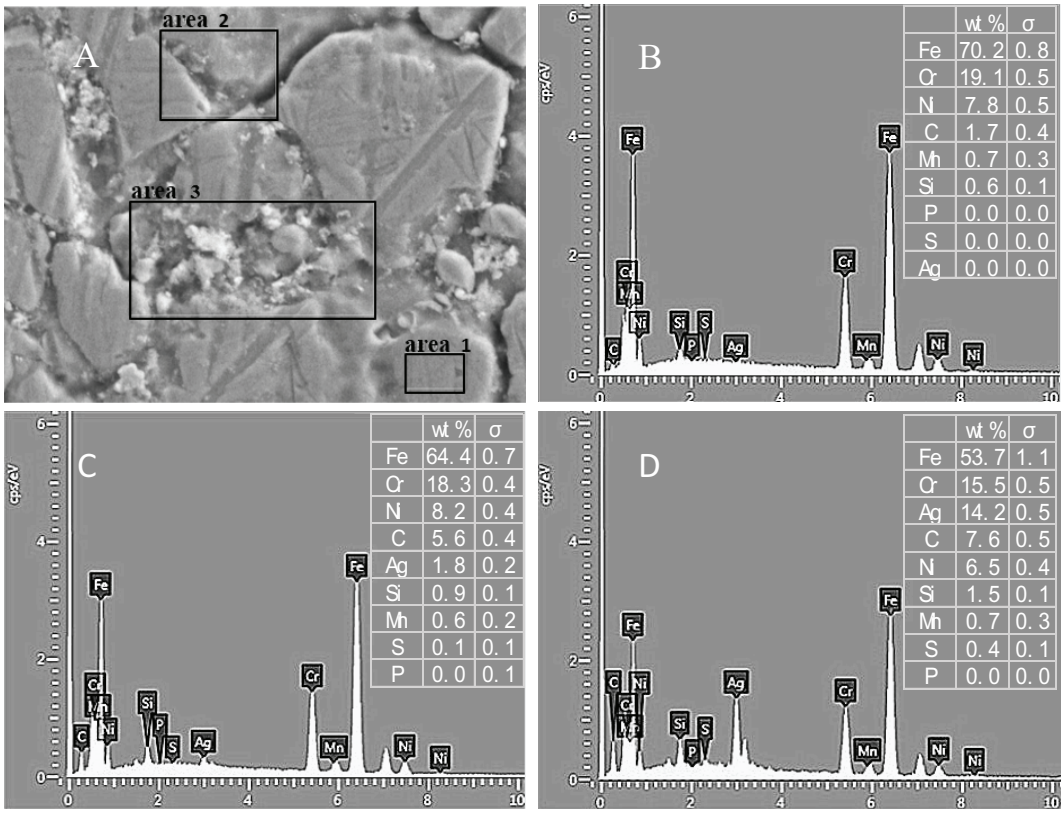

Fig. 2. EDS of the SS samples after adsorption. Panel A identifies the areas of analysis, marked 1 to 3, with their respective EDS findings shown in panels B–D.

3.1.2. Surface element analysis by X-ray photoelectron spectroscopy

XPS was also used to determine the Ag element on the surface of SS. The survey spectrum in the range of 0–1,200 eV recorded for SS before and after adsorption of silver nitrate, marked as SS and SS-Ag, respectively, is presented in Fig. 3. The spectral line of C1s (284.6 eV) was utilized to calibrated the binding energies. Although, Fe is the main component of SS, XPS, analysis produced a Fe peak with an intensity that was much lower than those of C and O peaks. Since XPS is a surface analysis technology, the sampling depth is generally between 1.5–9 nm for metal samples. The high intensity of the C and O peak were most likely due to surface contamination and these masked the characteristic Fe peak of SS.

The spectrum of SS-Ag following adsorption clearly produces an Ag3d peak. Thus, through XPS analysis, it was verified that the material adsorbed on the SS surface contained silver. From inset (b) in Fig. 3 it can be seen that the peaks of $Ag3d_{3/2}$ and $Ag3d_{5/2}$ had binding energies of about 374.2 and 368.2 eV respectively, which is consistent with the results of Zhou et al [17], and the slitting of the 3d doublet of Ag is 6.0 eV, suggesting the metallic nature of silver [18].

3.2. Influence of the contact time and the initial silver concentration

In order to investigate the effect of adsorption duration and initial silver concentration on the adsorption process, the SS adsorption capacity was measured at different time points and different initial concentrations of Ag^+ were compared. All experiments were performed at 45°C, and the results are shown in Fig. 4. The adsorption process started by rapid initial adsorption followed by a slower increase, while after 72 h equilibrium was reached. The initial rapid adsorption stage lasted for approximately 24 h, a slow adsorption stage was defined between 24–72 h, and an adsorption saturation stage could be recognized after 72 h.

Fig. 4(a) shows that the adsorption rate of Ag^+ was faster in the initial stage, so that after 24 h the adsorption capacity had reached more than half of the equilibrium adsorption capacity already. This indicates that the used SS had sufficient numbers of available surface adsorption sites and the concentration of Ag^+ in the solution was high enough to enable rapid adsorption [19]. With continued incubation, fewer adsorption sites on the SS surface were left available and the Ag^+ concentration in solution also gradually decreased, slowing down the adsorption rate. After 72 h, Ag^+ probably occupied most of the available adsorption sites on the surface, so that the adsorption process reached equilibrium.

When the initial concentration of Ag^+ increased, the equilibrium adsorption capacity also increased. Based on the data presented in Fig. 4(a), the adsorption capacity of SS increased from 29.307 (at an initial Ag^+ concentration of 0.4 mg/L) to 40.966 mg/m^2 starting with 1.2 mg/L Ag^+, representing an increase by approximately 28%. The initial rapid increase and the higher adsorption capacity at higher starting concentrations were due to the greater number of Ag^+ ions present in solution relative to the (fixed) number of available active sites on the sorbent surface. These higher initial concentrations could furthermore overcome the mass transfer resistance of Ag^+ to the SS surface more easily to enable adsorption. Similar findings were also demonstrated by Staron et al [19].

As shown in panel (b) of Fig. 4, with initial Ag^+ concentrations ranging from 0.4 to 1.2 mg/L, the removal rate at

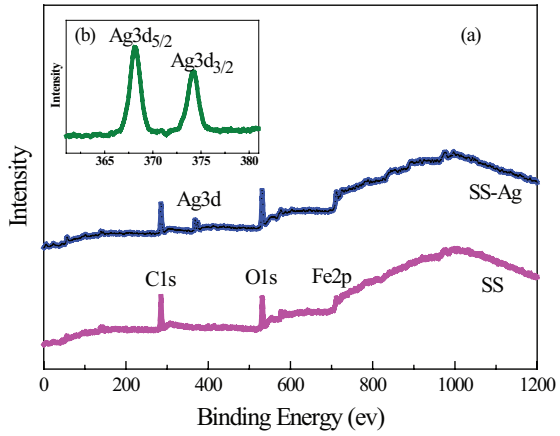

Fig. 3. XPS characterizations of SS samples before adsorption (SS) and after adsorption of silver (SS-Ag) (a); The inset (b) shows the energy binding of the silver peaks.

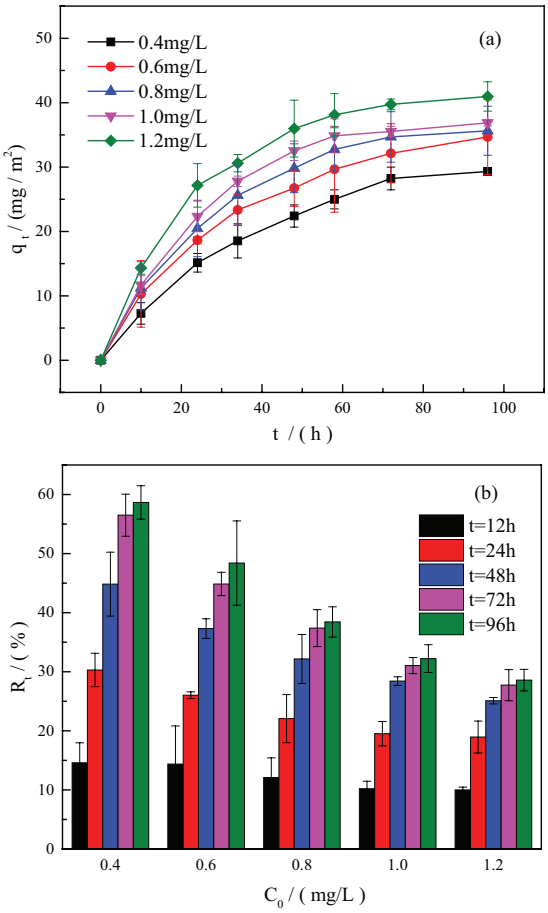

Fig. 4. Influence of initial silver concentration on adsorption capacity (a); and removal rate (b).

12 h was 14.60%, 14.37%, 12.10%, 10.20%, and 10.00%, respectively, with a slight but not significant difference between these initial concentrations. After longer incubations, the removal rate decreased significantly as the initial Ag^+ concentration raised. This may be related to the higher adsorption rate due to higher Ag^+ concentrations, as the effect of concentration on the removal rate was not significant. After 48 h, the increase in adsorption rate slowed down, and the initial concentration became the major factor affecting the removal rate. It was obvious that increasing the Ag^+ concentration in the solution with a constant number of available adsorption sites lowered the degree of relative removal as a result of the consuming the available active sites. Thus, when the adsorption process reached equilibrium, the relative Ag^+ removal rate at an initial concentration of 1.2 mg/L was the lowest (28.59%), which was a decrease of 30.08% compared with the removal rate (58.67%) obtained with a concentration of 0.4 mg/L.

3.3. Adsorption kinetics

The adsorption kinetics can provide valuable insights into the reaction pathways and offer information on the physical chemistry of the adsorption mechanism at play. In this study, four models were compared with describe the adsorption process of Ag^+ on SS: the pseudo first-order rate model [20], pseudo second-order rate model [21], Elovich model [22], and intra-particle diffusion model [23]. The parameters of these kinetic models with their correlation coefficient (R^2) are represented in Table 2.

The correlation coefficient (R^2) was used to compare models and their correlation at various concentrations and times. As seen from Table 2, the values of R^2 were relatively low based on the pseudo-first-order model and the experimental q_e values differed slightly from the corresponding values derived from the equation. Hence, the adsorption of Ag^+ onto SS did not follow the pseudo-first-order model, which suggested that the external diffusion was not the determining step in the adsorption process. Although, the first-order rate kinetic model has been widely used in various adsorption processes, it has some limitations, as it is more suitable to describe the kinetics of the initial adsorption stage, but cannot accurately describe the entire adsorption process [24]. This may be why R^2 of the pseudo first-order rate model (0.9012–0.9907) were lower than those of the pseudo-second order model. Conversely, the experimental data fitted best with the pseudo-second order kinetic model according to R^2 (0.9848–0.9986) values. Moreover, the pseudo second-order rate constant k_2 decreased with initial concentration, and this was also consistent with the experimental data. A graphical representation is shown in Supplementary Fig. S1. The results indicated that the rate-limiting step for the adsorption of Ag^+ on the SS surface was chemisorption, which was based on the interaction of valence forces through the sharing or exchange of electrons between Ag^+ and SS [21]. Hence, the pseudo-second order rate model better described the adsorption kinetics. Similar findings were reported for the adsorption of Ag^+ on activated carbon [25]. Additionally, although the Elovich model is an empirical equation and does predict any definite mechanism, it is useful in describing adsorption rate and concentration changes. As the Elovich constant α can represent the initial rate of adsorption, the SS demonstrated higher initial adsorption rate in high concentration of Ag^+ at the beginning of the adsorption experiments due to the higher α value. The Intra-particle diffusion model did not satisfyingly fit the experimental adsorption data as it produced the lowest correlation coefficients (R^2 ranged from 0.8859 to 0.9698).

3.4. Adsorption isotherm

Fitting the data representing the equilibrium state allows for more complete description of the process to elucidate the adsorption mechanism, as the adsorbate can be adsorbed from the aqueous solution onto the surface of the solid sorbent by several mechanisms. The adsorption isotherms express the specific relation between the concentration of adsorbate and its degree of accumulation onto an adsorbent surface at a constant temperature. In general, analytic forms of adsorption isotherms are complex due to differences in solid surface structure and energy distribution. In this study, four models

Table 2
Kinetic parameters of different adsorption models at different initial Ag^+ concentrations

Kinetics model	Parameters	C_0 (mg/L)				
		0.4	0.6	0.8	1.0	1.2
Pseudo first-order	q_e (mg/m^2)	36.478	36.244	43.128	41.196	44.441
	k_1 (h^{-1})	0.0415	0.0349	0.0478	0.0482	0.0477
	R^2	0.9012	0.9869	0.9622	0.9879	0.9907
Pseudo second-order	q_e (mg/m^2)	44.267	48.356	48.804	49.237	52.138
	k_2 (m^2/mg·h)	4.9×10^{-4}	5.5×10^{-4}	6.5×10^{-4}	7.2×10^{-4}	8.2×10^{-4}
	R^2	0.9912	0.9986	0.9913	0.9848	0.9938
Elovich	α (mg/m^2·h)	1.973	2.686	3.071	3.414	4.371
	β (m^2/mg)	0.0980	0.0904	0.0869	0.0848	0.0819
	R^2	0.9891	0.9956	0.9850	0.9711	0.9774
Intra-particle diffusion	I	–2.1230	0.2438	1.6960	3.0316	5.7316
	k_{id} (mg/m^2·h$^{0.5}$)	3.4500	3.7192	3.8161	3.8607	3.9968
	R^2	0.9656	0.9698	0.9275	0.8859	0.8915

were compared, Langmuir [26], Freundlich [27], Temkin [28], and Dubinin-Radushkevich (D-B) [29] to describe the adsorption of Ag on the SS surface. The results from fitting the model equations with their parameters and the resulting correlation coefficients are shown in Table 3. A graphical representation of the data is shown in Supplementary Fig. S2.

The Langmuir isotherm model produced the best fit of the experimental adsorption data, producing highest R^2 values. Moreover, the theoretical maximal adsorption capacity calculated by this model was 44.307 mg/m^2, which was close to the saturated adsorption capacity of 40.966 mg/m^2. Thus, the Langmuir isotherm model was the most suitable model to describe the adsorption equilibrium of Ag^+ on SS surfaces. Based on the Langmuir adsorption isotherm hypothesis, it can be inferred that Ag^+ adsorbed on SS forms a monolayer. Similar results were reported for the adsorption of Ag^+ on immobilized coffee ground beads and on Shenfu coal [30,31].

The essential characteristics of the Langmuir isotherm can be expressed in terms of a dimensionless constant separation factor (R_L). Eq. (7) shows the model on the basis of which R_L was calculated [32].

$$R_L = 1/\left(1 + bC_0\right) \tag{7}$$

There are four probable ranges for the value of R_L: A value in between 0 and 1 describes favorable adsorption; a value >1 describes unfavorable adsorption; for linear adsorption, $R_L = 1$; and for irreversible adsorption R_L equals 0.

The obtained R_L values were always positive and lower than 1 at 45°C, indicating that the adsorption of Ag^+ on SS is favorable at this temperature. With an increase of the initial Ag^+ concentration the R_L value approaches zero, which means that the adsorption becomes less favorable at high initial concentrations.

From the Freundlich isotherms, the exponent $1/n$ in the model is an indicator of adsorption favorability. In general, a value of heterogeneity factor (n) in the range of 2–10 means good, 1–2 moderately difficult, and less than 1 poor [33]. According to Table 3, the value of n (5.37) was between 2 and 10, implying the favorable adsorption process, which was in good agreement with the analysis of the separation factor (R_L). The value of n was higher than 1, also indicating that the adsorption energy decreases with increasing concentration for the adsorption of Ag^+ on SS [34]. The parameter E (equilibrium adsorption energy) of the D-R model could be used to determine the type of the adsorption process. The value of E (5.962 KJ/mol) was determined, outside the range of 8–16 kJ/mol, indicating that the adsorption type of Ag^+ on SS may be essentially physical [32]. The positive value of E obtained in the present study also indicated that the adsorption process was endothermic [27].

3.5. Thermodynamic analysis of the process

Temperature strongly affects the adsorption process, as it has a significant influence on the viscosity of the solution and on the mobility of metal ions in solution. The adsorption experiments were determined at five different temperatures (298, 308, 318, 328, and 338 K) with a constant pH of 6.5 and an initial Ag^+ concentration of 0.4 mg/L. The adsorption results obtained with these different temperatures are shown in Fig. 5. As expected, the adsorption capacity for Ag^+ was significantly higher with higher temperatures. When the temperature increased from 298 to 338 K, the equilibrium

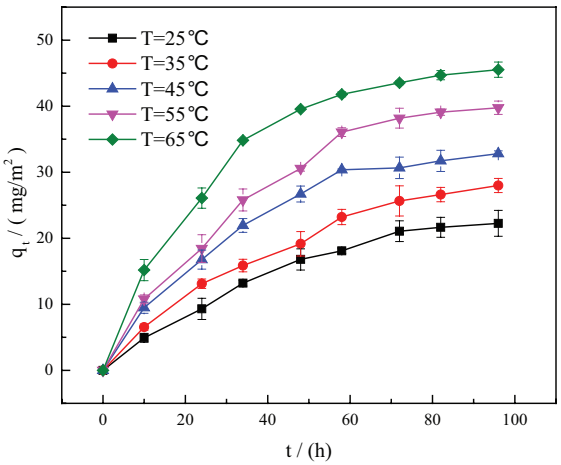

Fig. 5. Influence of temperature on the adsorption capacity.

Table 3
Parameters and the equations of the model at 45°C

Isotherm models	Linear fitting formula	Parameters	45°C
Langmuir	$y = 0.02257x + 0.00234$	q_{max} (mg/m^2)	44.307
		b (L/mg)	9.645
		R^2	0.9894
Freundlich	$y = 0.1863x + 1.61238$	k_f (mg$^{1-(1/n)}$L$^{1/n}$m^2)	40.962
		n	5.37
		R^2	0.9153
Temkin	$y = 6.43769x + 40.6459$	k_t (L/m^2)	552.106
		B (J/mol)	6.43769
		R^2	0.9107
Dubinin-Radushkevich	$y = -1.4067 \times 10^{-8}x + 3.72195$	E (KJ/mol)	5.962
		q_d (mg/m^2)	41.345
		R^2	0.8980

adsorption capacity increased from 22.25 to 45.52 mg/m^2, which confirmed that the adsorption of Ag^+ on SS surface was an endothermic process. At higher temperatures the adsorption rate was accelerated and the time required to reach adsorption equilibrium was shortened.

An understanding of the relevant thermodynamic parameters of the process is needed to establish if the adsorption process could occur spontaneously. Hence, the enthalpy change (ΔH), entropy change (ΔS), and Gibbs free energy (ΔG) were calculated using the following Eq. (8) and (9) [35]:

$$\Delta G = -RT\ln K_c \tag{8}$$

$$\ln K_c = \Delta SR - \Delta HRT \tag{9}$$

where R (8.314J·mol^{-1}·K^{-1}) is the universal gas constant, T (K) is the absolute temperature, and K_c is the distribution constant which is calculated from the ratio of the equilibrium concentration of Ag^+ on the adsorbent and in solution. ΔG (J/mol) is determined from Eq. (8), the values of ΔH (J/mol) and ΔS (J·mol^{-1}·K^{-1}) were calculated from the slope and intercept of the plots of ln K_c vs. 1/T (Fig. 6).

The calculated values of ΔG, ΔS, and ΔH are shown in Table 4. The negative value of ΔG indicates that the adsorption process is spontaneous. Moreover, the decrease in ΔG values along with an increased temperature suggests that the adsorption is more favorable at high temperature [36]. The ΔG values obtained in this study ranged between –20 and zero

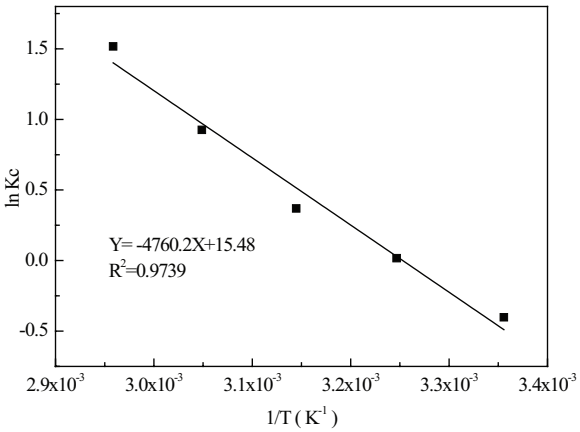

Fig. 6. Line graph for the determination of thermodynamic parameters.

Table 4
Thermodynamic parameters of adsorption process

C_{Ag} (mg/L)	T (K)	ΔG (KJ/mol)	ΔH (KJ/mol)	ΔS (J·mol^{-1}·K^{-1})
0.4	298	1.00	39.58	128.74
	308	–0.04		
	318	–0.98		
	328	–2.53		
	338	–4.26		

KJ.mol^{-1}, indicating that during the adsorption process novel chemical bonds were not formed, and the interaction forces may instead be electrostatic force, hydrogen bonding forces, hydrophobic distribution forces and Van der Waals' forces, all of which could be responsible for physical adsorption [37]. The positive value of ΔS suggested that the randomness of the solid/solution interface increased during the adsorption process. The positive value of ΔH indicated the endothermic nature of the adsorption process, which was in line with the results of D-R isothermal model.

3.6. Desorption

Fig. 7 shows the analytical results of eluted Ag^+ from the SS using various eluents. When ultra-pure water was used, no desorption took place, and desorption in tap water was also very weak. As there are few ions in ultra-pure water that can interact with Ag^+, desorption mostly depends on the mechanical force of the solution, and this appears to be insufficient to overcome the adsorption force between Ag^+ and the SS surface. Although tap water contains minor amounts of anions and cations, their concentration was too low to support desorption. Based on these results, it could be concluded that the adsorption force of Ag^+ and SS was relatively strong, and the shear action of the water flow inside a water pipe would not be sufficient to remove Ag^+. This suggested that the antibacterial performance of Ag^+ adsorbed on the inside of a water pipe might be maintained for a long time.

It was found that 0.1 mol/L sodium thiosulfate or 1% thiourea could effectively desorb Ag^+ from the SS surface, and their desorption rate reached 78.79% and 73.89% at 6 h, respectively. With an extension of the contact time, desorption rate increased slightly. Both sodium thiosulfate and thiourea cam form complexes with Ag^+, and their binding force was larger than the adsorption force between Ag^+ and the SS, which enabled effective desorption. Of the two tested salts, sodium thiosulfate resulted in more elution of Ag^+.

The concentration of the salts in the eluent has a significant influence on desorption. Fig. 8 shows the amount of the desorbed Ag^+ and removal rate in different $Na_2S_2O_3$

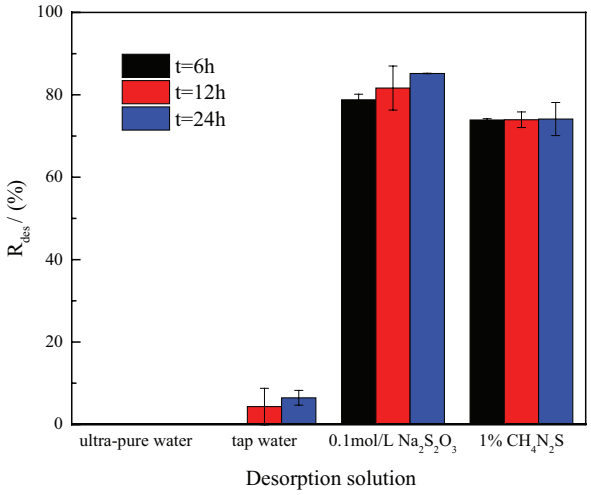

Fig. 7. Desorption of adsorbed Ag^+ using different solutes.

and CH_4N_2S concentrations. The desorbed amount of Ag^+ was higher at high salt concentrations but a concentration-dependent effect was not obvious at low salt concentrations. The eluent containing 0.25% or 0.5% CH_4N_2S produced similar results, with a desorption rate of 53.78% and 53.81%, respectively. In contrast, the desorption rate of 0.025 mg/L $Na_2S_2O_3$ solution was slightly larger than that of 0.5 mg/L. When the $Na_2S_2O_3$ concentration was increased to 2 mg/L, the desorption rate increased to 98.35%, so that desorption of the Ag^+ from the SS surface was almost complete. With CH_4N_2S concentrations reaching 0.5% or more, the desorption rate increased significantly, and the desorption rate of 2% CH_4N_2S was 93.53% at 24 h, which was slightly lower than that obtained with 2 mg/L $Na_2S_2O_3$.

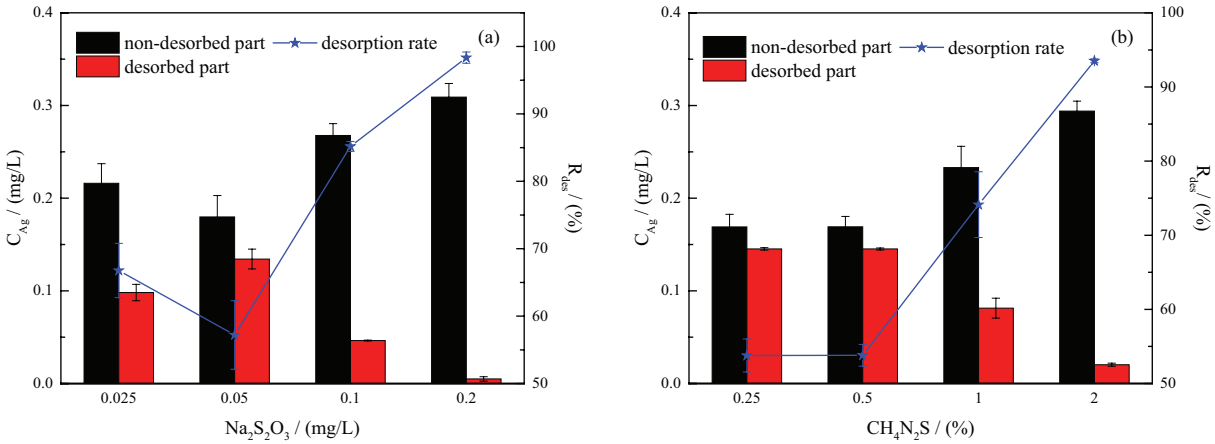

Fig. 8. Desorption effect in different concentrations of (a) $Na_2S_2O_3$, and (b) CH_4N_2S.

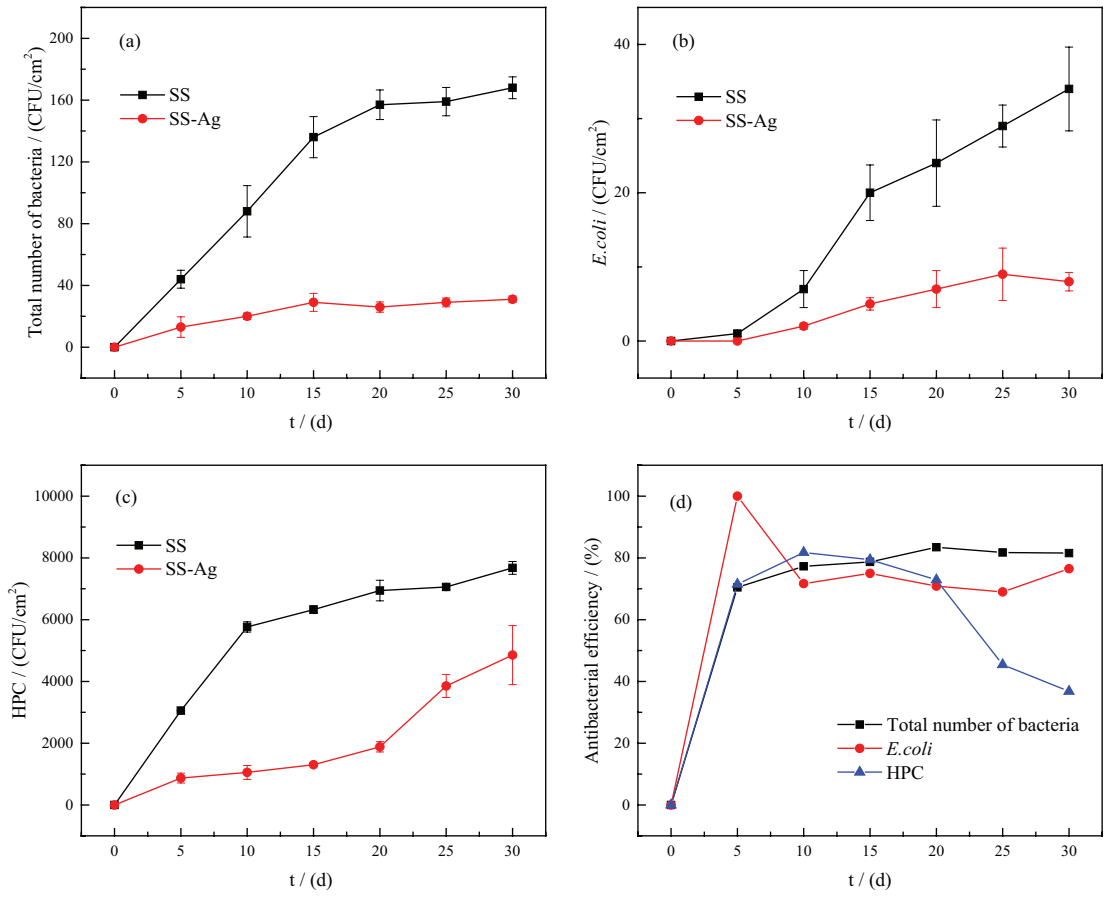

Fig. 9. Antibacterial activity of SS-Ag against total number of bacteria (a); *E. coli* (b) and HPC (c) in biofilm; and antibacterial efficiency of SS-Ag (d).

3.7. Antimicrobial properties

The biofilm inhibition ability of SS-Ag was assessed against total number of bacteria, *E. coli* and HPC as model microorganism and the results were shown in Fig. 9.

It can be seen from Fig. 9 that the quantity of bacteria on SS-Ag was much lower than SS coupon during the test period and the growth rate of microorganisms on SS surface was faster. SS-Ag had a relatively high antibacterial efficiency against total number of bacteria and *E. coli*, which still maintained at 60%–80% in the case of water pollution. As for HPC, the antibacterial efficiency within 20 d was also in this range, but decreased significantly after 20 d. SS-Ag had a certain antibacterial effect on all of model bacteria in study, which fully reflected the broad-spectrum antibacterial activity of silver. It can be inferred that the adsorption of Ag^+ on the surface of SS improved antibacterial activity and prevented the formation of biofilm, which would be beneficial for long-term treatment of domestic hot water.

It can be observed that a large amount of biofilm was formed on SS and increased significantly with time. This is mainly due to the fact that SS coupons unable to prevent the growth of bacteria and the cells attached on them with time leading to the formation of biofilm. In contrast, the biofilm formation was inhibited to a certain extent on SS-Ag coupon surface. Silver content in BAR effluent was lower than detection limit during the test period, indicating the silver desorption in water was very weak. The phenomenon was in good agreement with desorption test results. Therefore, it can be inferred that direct contact of SS-Ag coupon with bacteria inhibited its growth and prevented biofilm formation. Dang et al [38] studied the antibacterial effect of silver nanoparticle containing silica beads, and suggested that the *E. coli* were killed by contacting with silver nanoparticles located on the surface of silica beads, which was similar to our research. Other studies also showed that silver nanoparticles containing materials can inhibit the biofilm formation, and had great cell-killing effect [39,40]. Both AgNPs and silver have good antibacterial properties. AgNPs can effectively avoid pore clogging and have little effect on the adsorption capacity of materials. Metal pipes are not porous materials, and it is more convenient to absorb Ag^+ to achieve antimicrobial effect. AgNPs containing porous materials are widely used in primary disinfection of water. The adsorption capacity of metal pipe wall to Ag^+ is lower than that of porous material, but it can ensure the safety of domestic hot water quality and effectively avoid secondary pollution in the supply process.

4. Conclusions

This study used an experimental model to show that the use of Ag^+ for emergency and shock disinfection of domestic hot water would most probably result in the adsorption of Ag^+ on the inner surface of a SS water pipe. The degree of adsorption established under experimental conditions depended on contact time, initial concentration of Ag^+ and temperature. Adsorption kinetic studies showed that the adsorption of Ag^+ SS was best described by the pseudo-second order model. On this basis, it was assumed that the adsorption was of a chemical nature. The adsorption isotherm could be fitted well in the Langmuir model ($R^2 = 0.9894$), and the maximum adsorption capacity reached 44.307 mg/m^2 at temperatures of 45°C. It was inferred that the Ag^+ adsorbed on the SS formed a monolayer. Thermodynamic studies confirmed that the adsorption occurred as an endothermic, feasible, and spontaneous process.

The desorption results presented here showed that ultrapure water could not desorb Ag^+ from the SS, and the desorption effect of tap water was also very weak. This suggests that the adsorption forces of Ag^+ and SS were strong, and that shear action of a typical water flow inside a water pipe would not lead to a significant removal of Ag^+. Therefore, the antibacterial performance of Ag^+ adsorbed on the inside of a pipe wall could maintain for a long time. Solutions of $Na_2S_2O_3$ and CH_4N_2S could effectively desorb Ag^+ from the SS surface, with nearly complete desorption obtained with 2 mg/L $Na_2S_2O_3$.

Antibacterial experiments showed that the quantity of microorganisms in biofilm of SS-Ag was much lower than SS during the test period. The adsorption of Ag^+ on SS improved its antibacterial activity and inhibited the formation of biofilm. SS-Ag had long-term antibacterial effect and reduced the risk of secondary pollution during domestic hot water supply process.

Acknowledgments

This work was financially supported by the National Water Pollution Control and Treatment Science and Technology Major Project in China (2014ZX07406002) and National Key R&D Program of China (2018YFC0406203). We would like to give our sincere thanks to the peer-reviews for their suggestions.

References

[1] P.M. Armstrong, M. Uapipatanakul, I. Thompson, D. Ager, M. McCulloch, Thermal and sanitary performance of domestic hot water cylinders: conflicting requirements, Appl. Energ., 131 (2014) 171–179.
[2] L.K. Bagh, H. Albrechtsen, E. Arvin, K. Ovesen, Distribution of bacteria in a domestic hot water system in a Danish apartment building, Water Res., 38 (2004) 225–235.
[3] P. Borella, M.T. Montagna, V. Romano-Spica, S. Stampi, G. Stancanelli, M. Triassi, R. Neglia, I. Marchesi, G.D. Tato, C. Napoli, G. Quaranta, P. Laurenti, E. Leoni, G.D. Luca, C. Ossi, M. Moro, G.R. Dalcala, Legionella infection risk from domestic hot water, Emerg. Infect. Dis., 10 (2004) 457–464.
[4] M.J. Nieuwenhuijsen, M. David, G. James, B. James, N.B. Nicky, I. Nina, V. Martine, B.T. Mireille, Chlorination disinfection by-products in drinking water and congenital anomalies: review and meta-analyses, Environ. Health. Persp., 117 (2009) 1486–1493.
[5] P. Roccaro, H. Chang, F.G. Vagliasindi, G.V. Korshin, Differential absorbance study of effects of temperature on chlorine consumption and formation of disinfection by-products in chlorinated water, Water Res., 42 (2008) 1879–1888.
[6] Y. Choi, Y.J. Choi, The effects of UV disinfection on drinking water quality in distribution systems, Water Res., 44 (2010) 115–122.
[7] S.P. Pathak, K. Gopal, Evaluation of bactericidal efficacy of silver ions on Escherichia coli for drinking water disinfection, Environ. Sci. Pollut. R., 19 (2012) 2285–2290.
[8] Q.L. Feng, J. Wu, G.Q. Chen, F.Z. Cui, T.N. Kim, J.O. Kim, A mechanistic study of the antibacterial effect of silver ions on Escherichia coli and Staphylococcus aureus, J. Biomed. Mater. Res., 52 (2000) 662–668.

[9] A.D. Russell, W.B. Hugo, 7 Antimicrobial Activity and Action of Silver, Prog. Med. Chem., 31 (1994) 351–370.
[10] Y. Inoue, M. Hoshino, H. Takahashi, T. Noguchi, T. Murata, Y. Kanzaki, H. Hamashima, M. Sasatsu, Bactericidal activity of Ag–zeolite mediated by reactive oxygen species under aerated conditions, J. Inorg. Biochem., 92 (2002) 37–42.
[11] T.Q. Tuan, N.V. Son, H.T.K. Dung, N.H. Luong, B.T. Thuy, N.T.V. Anh, N.D. Hoa, N.H. Hai, Preparation and properties of silver nanoparticles loaded in activated carbon for biological and environmental applications, J. Hazard. Mater., 192 (2011) 1321–1329.
[12] E. Altintig, G. Arabaci, H. Altundag, Preparation and characterization of the antibacterial efficiency of silver loaded activated carbon from corncobs, Surf. Coat. Tec., 304 (2016) 63–67.
[13] Y. Ma, T. Zhou, C. Zhao, Preparation of chitosan-nylon-6 blended membranes containing silver ions as antibacterial materials, Carbohyd. Res., 343 (2008) 230–237.
[14] H. Lu, J. Wang, M. Stoller, T. Wang, Y. Bao, H. Hao, An overview of nanomaterials for water and wastewater treatment, Adv. Mater. Sci. Eng, 2016 (2016) 1–10.
[15] D.V. Halem, H.V.D. Laan, S.G.J. Heijman, J.C.V. Dijk, G.L. Amy, Assessing the sustainability of the silver-impregnated ceramic pot filter for low-cost household drinking water treatment, Phys. Chem. Earth., 34 (2009) 36–42.
[16] N. Silvestry-Rodriguez, K.R. Bright, D.C. Slack, D.R. Uhlmann, A.C.P. Gerba, Silver as a residual disinfectant to prevent biofilm formation in water distribution systems, Appl. Environ. Microb., 74 (2008) 1639–1641.
[17] X. Zhou, C. Wang, H. Huang, X. Ji, B. Wu, Extensive adsorption of the lighter homologue tellurium of polonium from wastewater using porous silver layer deposited stainless steel mesh, Prog. Nucl. Energ., 98 (2017) 285–292.
[18] M. Petala, V. Tsiridis, I. Mintsouli, N. Pliatsikas, T. Spanos, P. Rebeyre, E. Darakas, P. Patsalas, G. Vourlias, M. Kostoglou, S. Sotiropoulos, T. Karapantsios, Silver deposition on stainless steel container surfaces in contact with disinfectant silver aqueous solutions, Appl. Surf. Sci., 396 (2017) 1067–1075.
[19] P. Staroń, J. Chwastowski, M. Banach, Sorption and desorption studies on silver ions from aqueous solution by coconut fiber, J. Cleaner. Prod., 149 (2017) 290–301.
[20] M. Yoosefian, S. Ahmadzadeh, M. Aghasi, M. Dolatabadi, Optimization of electrocoagulation process for efficient removal of ciprofloxacin antibiotic using iron electrode; kinetic and isotherm studies of adsorption, J. Mol. Liq., 225 (2017) 544–553.
[21] Y.S. Ho, G. Mckay, Pseudo-Second Order Model for Sorption Process, Process Biochem., 34 (1999) 451–465.
[22] H.I. Inyang, A. Onwawoma, S. Bae, The Elovich equation as a predictor of lead and cadmium sorption rates on contaminant barrier minerals, Soil. Tillage. Res., 155 (2016) 124–132.
[23] A.M.K. Pandian, C. Karthikeyan, M. Rajasimman, Isotherm and kinetic studies on nano-sorption of malachite green onto Aspergillus flavus mediated synthesis of silver nano particles, Biocatal. Agric. Biotechnol., 8 (2016) 171–181.
[24] Y. Li, Q. Yue, B. Gao, J. Yang, Y. Zheng, Adsorption kinetics of reactive dyes on activated carbon fiber, Environ. Sci., 28 (2007) 2637–2641.
[25] X. Song, P. Gunawan, R. Jiang, S.S.J. Leong, K. Wang, R. Xu, Surface activated carbon nanospheres for fast adsorption of silver ions from aqueous solutions, J. Hazard. Mater., 194 (2011) 162–168.
[26] A.O. Dada, Langmuir, Freundlich, Temkin and Dubinin–Radushkevich isotherms studies of equilibrium sorption of Zn^{2+} unto phosphoric acid modified rice husk, Russ. J. Appl. Chem., 3 (2012) 38–45.
[27] S.M. Mousa, N.S. Ammar, H.A. Ibrahim, Removal of lead ions using hydroxyapatite nano-material prepared from phosphogypsum waste, J. Saudi Chem. Soc., 20 (2016) 357–365.
[28] M.J. Temkin, V. Pyzhev, Recent modifications to Langmuir isotherms, Acta Physiochim URSS, 12 (1940) 217–222.
[29] H.D. Setiabudi, R. Jusoh, S.F.R.M. Suhaimi, S.F. Masrur, Adsorption of methylene blue onto oil palm (*Elaeis guineensis*) leaves: process optimization, isotherm, kinetics and thermodynamic studies, J. Taiwan Inst. Chem. Eng., 63 (2016) 363–370.
[30] C. Jeon, J.H. Cha, J.Y. Choi, Adsorption and recovery of immobilized coffee ground beads for silver ions from industrial wastewater, J. Ind. Eng. Chem., 53 (2017) 261–267.
[31] Z. Yu, A. Zhou, J. Qu, T. Zhang, Study on behavior and kinetics of sorption of Ag^{+} by Shenfu3^{-1} coal, Microporous. Mesorporous. Mater., 85 (2005) 104–110.
[32] H. Zheng, D. Liu, Y. Zheng, S. Liang, Z. Liu, Sorption isotherm and kinetic modeling of aniline on Cr-bentonite, J. Hazard. Mater., 167 (2009) 141–147.
[33] X. Li, J. Wang, X. Zhang, C. Chen, Powdered activated carbon adsorption of two fishy odorants in water: trans,trans-2,4-heptadienal and trans,trans-2,4-decadienal, J. Environ. Sci.-China, 32 (2015) 15–25.
[34] N. Can, B.C. Mür, A. Altndal, Modeling of heavy metal ion adsorption isotherms onto metallophthalocyanine film, Sens. Actuators, B, 237 (2016) 953–961.
[35] C. Pradeep Sekhar, S. Kalidhasan, V. Rajesh, N. Rajesh, Biopolymer adsorbent for the removal of malachite green from aqueous solution, Chemosphere., 77 (2009) 842–847.
[36] Lutfullah, M. Rashid, U. Haseen, N. Rahman, An advanced Cr(III) selective nano-composite cation exchanger: synthesis, characterization and sorption characteristics, J. Ind. Eng. Chem., 20 (2014) 809–817.
[37] Z. Sun, B. Yan, A. Wang, N. Bai, Y. Li, Adsorption of reactive red X-3B on chitosan/CTAB modified bentonite, Acta Scien. Circum., 37 (2017) 617–623.
[38] D.V. Quang, P.B. Sarawade, S.J. Jeon, S.H. Kim, J. Kim, Y.G. Chai, H.T. Kim, Effective water disinfection using silver nanoparticle containing silica beads, Appl. Surf. Sci., 266 (2013) 280–287.
[39] P. Biswas, R. Bandyopadhyaya, Water disinfection using silver nanoparticle impregnated activated carbon: escherichia coli cell-killing in batch and continuous packed column operation over a long duration, Water Res., 100 (2016) 105–115.
[40] B. Ramalingam, M.M.R. Khan, B. Mondal, A.B. Mandal, S.K. Das, Facile synthesis of silver nanoparticles decorated magnetic-chitosan microsphere for efficient removal of dyes and microbial contaminants, ACS. Sustainable. Chem. Eng., 3 (2015) 2291–2302.

Supplementary material

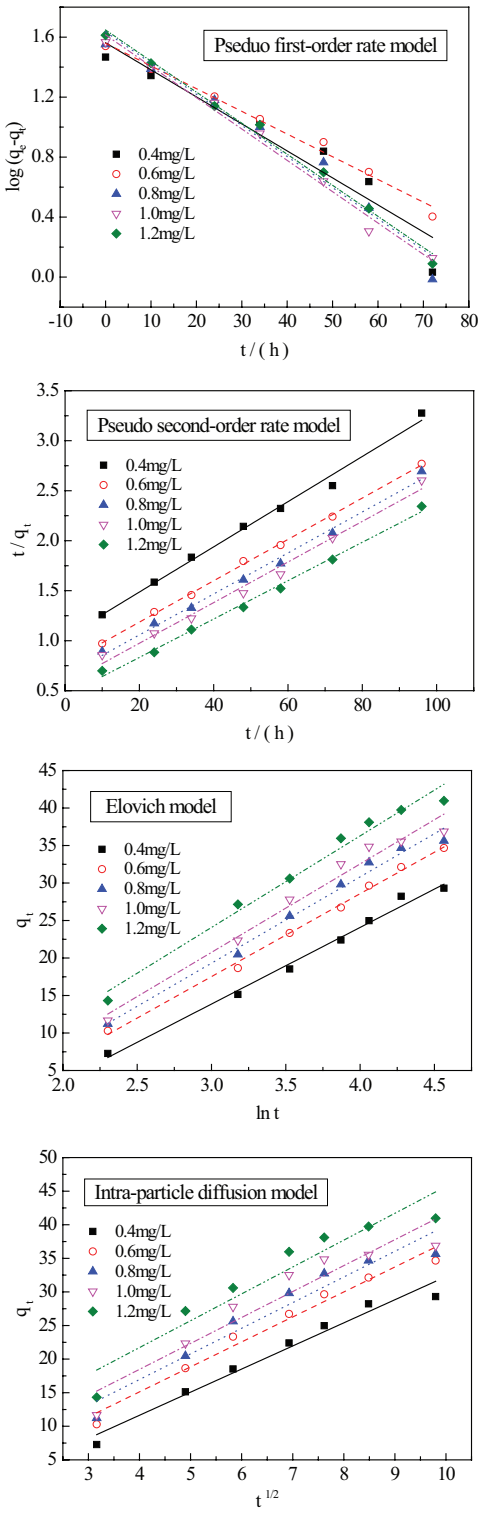

Fig. S1. Linear representation of the data fitted into the different models of sorption kinetics.

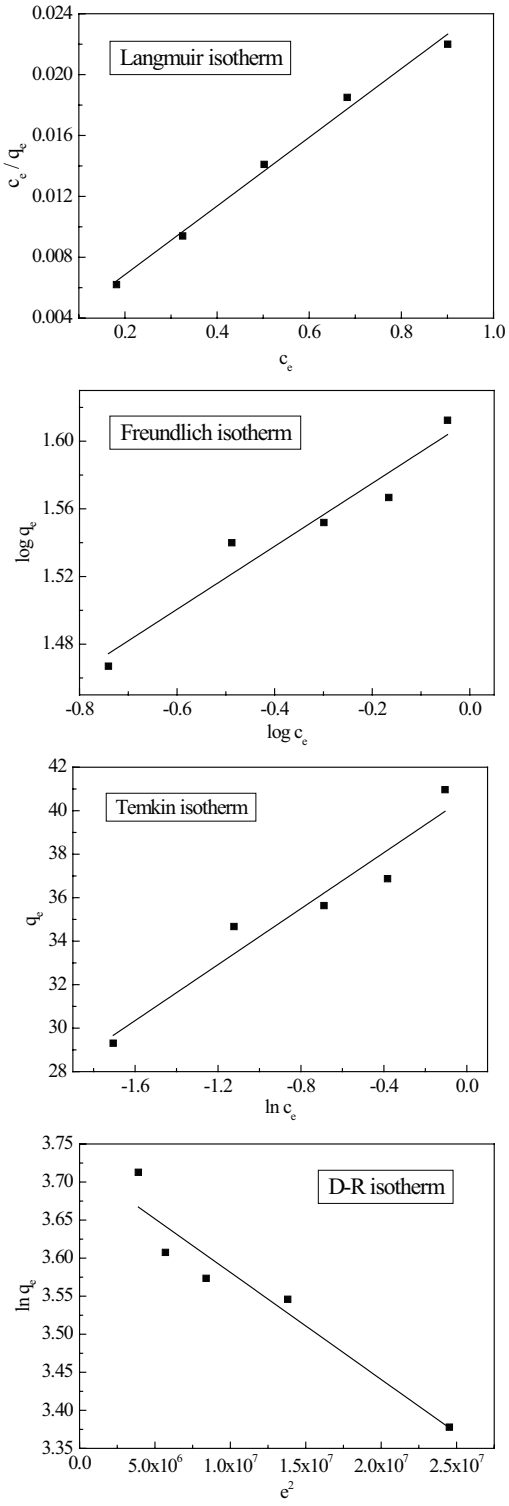

Fig. S2. Linear representation of the different models of sorption isotherms.